**CMO6** **2:45 pm**

## Low noise image amplification by contradirectional two-wave mixing in Rh-doped $BaTiO_3$ crystal

Xiaodong Mu, Xinguang Xu,*
Zongshu Shao,* Minhua Jiang,*
Haosu Luo,** *National Key Laboratory of Crystal Materials, Shandong University, Jinan 250100, China*

Most of the research on the photorefractive image amplification in the past adopted the configuration of forward two-wave mixing (FTWM). However, the beam fanning effect, a kind of forward stimulated photorefractive scattering (SPS), usually leads the amplified image to a poor signal-to-noise ratio (SNR).[1–5] In this report, we found contradirectional two-wave mixing (CTWM) can effectively remove the noise in the amplified image and can raise the gain.

For comparison, both of the configurations of FTWM and CTWM were investigated in our experiment. The extraordinary polarized pump and signal beams from a He-Ne laser entered the crystal as shown in Figs. 1(a) and 1(b) for FTWM and CTWM, respectively. The initial power ratio of pump and signal beams is $7 \times 10^4$. The dimensions of the $BaTiO_3$ crystal are 8.4 mm × 7.5 mm × 7.0 mm with the c-axis along the 7.0 mm edge. The Rh-doping concentration is about 218 ppm.

The original image and the amplified image

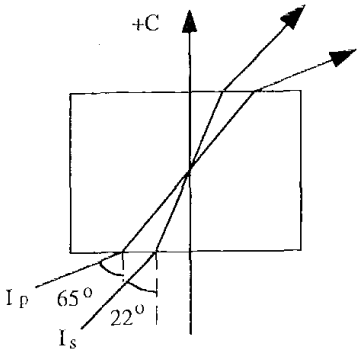


**CMO6 Fig. 1.** Scheme of (a) FTWM and (b) CTWM.

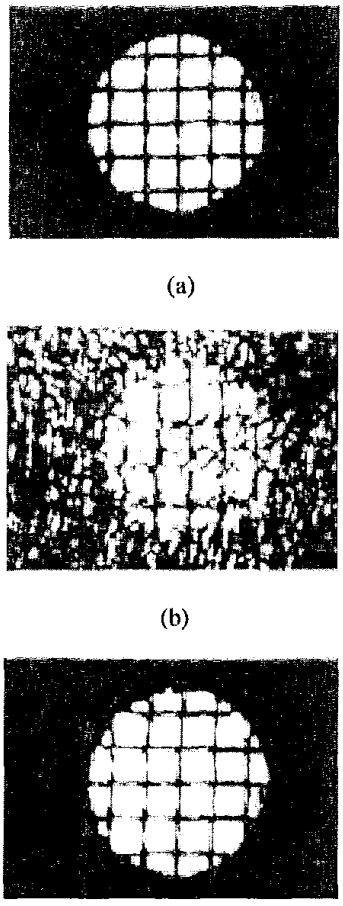


**CMO6 Fig. 2.** Comparison between the amplified images in the CTWM and FTWM schemes. (a) Input image. (b) Amplified image (6000×) by FTWM scheme. (c) Amplified image (10000×) by CTWM scheme.

by FTWM and by CTWM are shown in Figs. 2(a), 2(b) and 2(c), respectively. As reported previously,[1–3] the image in Fig. 2(b) is submerged in the noise from the beam fanning. However, the image in Fig. 2(c) is very clear. At the steady state, the measured SNR and gain are about 6 and $6 \times 10^3$ for FTWM and $2 \times 10^4$ and $1 \times 10^4$ for CTWM, respectively. Here, the SNR and gain (g) were calculated by the following equations[2]:

$$\mathrm{SNR} = \frac{I_S - I_N}{I_N}, \tag{1}$$

$$g = \frac{I_S - I_N}{I_{S0}}, \tag{2}$$

where $I_{S0}$ is the initial signal power behind the crystal; $I_S$ is the total power of the amplified signal beam and the noise; $I_N$ is the noise power that can be defined as the power of the SPS along the signal beam direction when the signal beam has been cut off and the gratings formed by signal and pump beams have been erased.

The above experimental results clearly show that the image amplified by CTWM has a much better quality and higher gain than that by FTWM. We believe this is due to the following advantages of CTWM. Firstly, the forward-going beam fanning from the pump beam can not affect the backward-going signal beam in the CTWM scheme. Secondly, the backward SPS from the pump beam can be eliminated automatically at the steady-state because CTWM has a smaller coupling constant than FTWM.[6] Figure 3 is the measured time evolution of the total power of the forward and backward SPS from the pump beam. One can see that the backward SPS power is lower than the forward SPS power by three orders of magnitudes. Furthermore, the backward SPS is erased after the forming of the beam fanning. Finally, the CTWM scheme does not need all of the optical energy to pass through the whole crystal. The most of pump energy can be brought out by the signal after a very short trip.[6] Therefore, the CTWM scheme reduces the losses caused by absorption and SPS, which leads to a higher gain in the CTWM scheme.

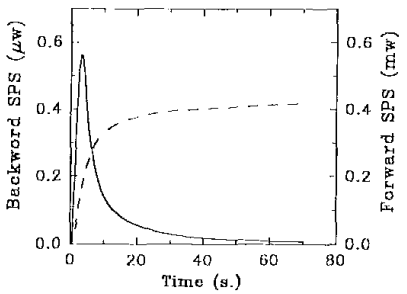


**CMO6 Fig. 3.** Time evolution of the SPS powers. The solid and dashed curves correspond to the backward and forward SPS.

*Shandong Univ., China
**Shanghai Inst. of Ceramics, Academia Sinica, China

1. H. Rajbenbach, A. Delbulbe, J.-P. Huignard, Opt. Lett. **14,** 1275 (1989); **16,** 1481 (1991).
2. J. Joseph, P.K.C. Pillai, K. Singh, Opt. Commun. **80,** 84 (1990); Appl. Opt. **30,** 3315–3318 (1991).
3. S. Breugnot, D. Dolfi, H. Rajbenbach, J.-P. Huignard, M. Defour, Opt. Lett. **19,** 1070 (1994).
4. D.B. He and P. Yeh, Appl. Opt. **33,** 283 (1994).
5. Z. Zhang, X. Ding, Y. Zhu, Q. Jiang, X. Mi, Z. Yu, P. Fu, Opt. Commun. **97,** 105 (1993).
6. X. Mu, X. Xu, Z. Shao, M. Jiang, H. Luo, W. Zhong, Appl. Phys. Lett. **71,** 1011 (1997).

**CMO7** **3:00 pm**

## Doping effects in polarization switching of lithium niobates

L.-H. Peng, Y.-C. Zhang, Y.-C. Lin, *Inst. of Electro-Optical Engineering, National Taiwan Univ., Taipei, 106 Taiwan, R.O.C.; E-mail: peng@cc.ee.ntu.edu.tw*

Quasi-phase-matching (QPM) of ferroelectric nonlinear optical crystals with periodi-

cally 180° inverted domain structures has merged as an important technology for nonlinear frequency generation. A plethora of research activity in nonlinear optics has benefited from the availability of periodically poled lithium niobate (PPLN) and lithium tantalate (PPLT) as the source for infrared optical parametric and harmonic generation. Great challenge, however, resides in manipulating the coercive field required for polarization switching such that high fidelity of fine QPM structure can be maintained in the course of frequency conversion.[1]

By far, common practice has regarded the congruent grown lithium niobate ($LiNbO_3$) and lithium tantalate ($LiTaO_3$) as the cost-effective materials for fabricating QPM devices despite the enormously large coercive field (>20 kV/mm) and internal field (>3 kV/mm) associated with the non-stoichiometric crystal growth.[2] It has been recently noted that 4 ~ 5 times and 14 times reduction in the polarization switching field, respectively, can be achieved by growing stoichiometric crystals of $LiNbO_3$ and $LiTaO_3$. However, the stoichiometric grown $LiNbO_3$ crystal has turned out to have lower optical damage threshold than the congruent grown one. Low level of magnesium oxide (MgO) doping is hence desired to suppress the optical damage.[3] In this work we report an investigation of the zinc oxide (ZnO) doping effects on the periodical poling process of congruent grown $LiNbO_3$ crystals. It is found by increasing the ZnO doping level up to 8 mol.%, the polarization switching field in ZnO:$LiNbO_3$ can drop down to 2.5 kV/mm with an internal field strength reduced to ~0.5 kV/mm. We thereby are able to not only reduce the polarization switching field in congruent grown $LiNbO_3$ crystals by one order of magnitude, but also minimize the corresponding axial anisotropy in the periodical poling process for the first time to our knowledge. We attribute the latter to an effective suppression of the crystal non-stoichiometry by ZnO doping in reducing the density of vacancy and the anti-site point defects.

The Z-cut, 500-μm-thick congruent grown ZnO:$LiNbO_3$ substrates used in this study were diced into 1 cm × 1 cm squares and had a patterned area of 10 $mm^2$ contacted to the lithium chloride liquid electrodes. The ZnO doping level investigated in this study was varied from 5 mol % to 8 mol. %. In order to stabilize the domain reversal process, a fast turn-on, high peak reverse voltage bearable rectifying diode was in series with the poling apparatus such that relaxation of the inverted domain can be suppressed at the termination of high voltage pulsed field poling.

Shown in Fig. 1 are the (a) field ($E$) dependence of the polarization switching rate ($1/t_s$) on 5 mol.% ZnO:$LiNbO_3$, and (b) wave forms of polarization switching currents on various (5 ~ 8 mol.%) ZnO:$LiNbO_3$ in a *forward* (3.5 kV) and a *reverse* (2.9 kV) poling case, respectively. The linear dependence of $1/t_s$ on $E$ is found to be independent of the poling direction. It signifies an apparent sidewise domain motion in the high field regime. The axial anisotropy in the lateral sweeping rate of the 180° inverted domain motion can be characterized by the equation of $v_s = \mu_s[E - (E_{th} \pm E_{int})]$,

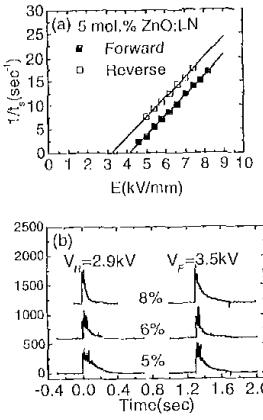


**CMO7 Fig. 1.** Field dependence of the (a) polarization switching rate, and (b) wave forms of the switching current in the forward and reverse poling direction on various ZnO-doped $LiNbO_3$ substrates.

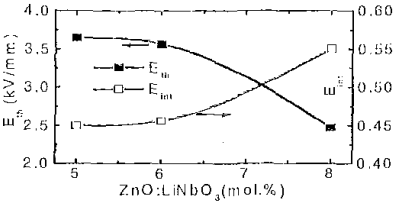


**CMO7 Fig. 2.** The ZnO doping dependence of threshold field and internal field in congruent grown $LiNbO_3$.

upon which a threshold field $E_{th}$ and an internal field $E_{int}$ of 3.6 kV/mm and 0.45 kV/mm, respectively, can be identified for the case of 5 mol.% ZnO:$LiNbO_3$. In the mobility model analysis shown above, the + (−) sign in ($E_{th} \pm E_{int}$) refers to the case of forward and reverse poling, respectively.[4] We also note from Fig. 1(b) that the polarization switching current and sweeping rate increase with the ZnO doping such that a higher ZnO doping results in a shorter switching time.

Shown in Fig. 2 are the measured $E_{th}$ and $E_{int}$ dependence on the ZnO doping in the congruent grown $LiNbO_3$ substrates. The data are obtained by measuring the field dependence of the polarization switching current and the corresponding waveform in the forward and reverse poling direction similar to those shown in Fig. 1, and by fitting with the mobility model analysis. We first note a dramatic decrease of $E_{th}$ down to 2.5 kV/mm with the increase of ZnO doping to 8 mol.%. It is worth comparing with the $E_{th}$ value of 17.6 kV/mm in the case of undoped congruent grown $LiNbO_3$.[4] Correspondingly, the $E_{int}$ also drops by one order of magnitude and reaches a value of 0.5 kV/mm. We attributed these observations to the effective suppression of the crystal's non-stoichiometry by the ZnO doping in reducing the density of vacancy and the anti-site point defects. In applying the ZnO doping method to control the periodical poling process of $LiNbO_3$, we illustrate in Fig. 3 a 5 mol.% ZnO:PPLN whose periodicity was designed to be 20 μm. Albeit it is *forward* poled at

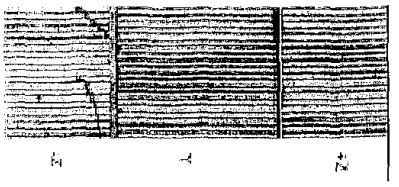

**CMO7 Fig. 3.** Cross-sectional view of the 5 mol.% ZnO:PPLN *forward* poled at 5 kV/mm.

a much smaller field of ~10 kV/mm, a good control of the aspect ratio is preserved over the 3-mm sample length and across the 500-μm-thick substrate.

In summary, we have found ZnO an efficient doping in reducing the switching and internal field on the congruent grown $LiNbO_3$ substrates. The observations of one order of magnitude reduction in these fields are attributed to an effective suppression of the crystal non-stoichiometry by the ZnO doping in reducing the density of vacancy and the anti-site point defects.


1. R.G. Batchko, V.Y. Shur, M.M. Fejer, R.L. Byer, "Backswitch poling in lithium niobate for high-fidelity domain patterning and efficient blue light generation," Appl. Phys. Lett. **75**, 1673–1675 (1999).
2. V. Gopalan, T.E. Mitchell, K.E. Sicakfus, "Switching kinetics of 180° domains in congruent grown $LiNbO_3$ and $LiTaO_3$ crystals," Solid State Commun. **109**, 111–117 (1999).
3. K. Kitamura, Y. Furukawa, S. Takekawa, K. Niwa, H. Hatano, "High optical damage resistance of near stoichiometric $LiNbO_3$ crystals with low level MgO doping," in *CLEO'99*, p. 446–447, paper CThM3, May 1999, Baltimore, MD.
4. L.-H. Peng, Y.-C. Fang, Y.-C. Lin, "Polarization switching of lithium niobate with giant internal field," Appl. Phys. Lett. **74**, 2070–2071 (1999).


## CMP

**1:30 pm–3:30 pm**
Room 103

### Pulsed Fiber Lasers

Yan Sun, *Lucent Tech., Bell Labs., USA, Presider*

**CMP1** **1:30 pm**

### Designs for efficient high-energy high brightness Q-switched cladding-pumped ytterbium-doped fiber lasers


C.C. Renaud, H.L. Offerhaus, J.A. Alvarez-Chavez, J. Nilsson, P.W. Turner, W.A. Clarkson, A.B. Grudinin, *Optoelectronics Res. Centre, Univ. of Southampton, Southampton SO17 1BJ, United Kingdom; E-mail: ccr@orc.soton.ac.uk*


Double-clad rare-earth-doped fiber lasers pumped by high brightness laser diodes are very efficient and compact sources of cw and